Nanoscale

PAPER

View Article Online
View Journal | View Issue

Cite this: *Nanoscale*, 2024, **16**, 8369

Orientation and morphology control in acid-catalyzed covalent organic framework thin films†

Dayanni D. Bhagwandin, [a,b] Kirt A. Page, [a,b,c] Ly D. Tran,[a,b] Yao Yao,[d] Alexander Reidell, [a,b] Christopher Muratore,[e] Qiyi Fang,[f,g] Aleksey Ruditskiy,[a,b] Cheri M. Hampton, [a,b] W. Joshua Kennedy, [a] Lawrence F. Drummy,[a] Yu Zhong,[g] Tobin J. Marks, [d] Antonio Facchetti, [d,h] Jun Lou, [f] Hilmar Koerner,[a] Luke A. Baldwin [a] and Nicholas R. Glavin *[a]

As thin films of semiconducting covalent organic frameworks (COFs) are demonstrating utility for ambipolar electronics, channel materials in organic electrochemical transistors (OECTs), and broadband photodetectors, control and modulation of their thin film properties is paramount. In this work, an interfacial growth technique is utilized to synthesize imine TAPB-PDA COF films at both the liquid–liquid interface as well as at the liquid–solid interface on a Si/SiO_2 substrate. The concentration of acetic acid catalyst in the aqueous phase is shown to significantly influence the thin film morphology of the liquid–solid growth, with concentrations below 1 M resulting in no film nucleation, concentrations of 1–4 M enabling smooth film formation, and concentrations greater than 4 M resulting in films with a higher density of particulates on the surface. Importantly, while the films grown at the liquid–liquid interface are mixed-orientation, those grown directly at the liquid–solid interface on the Si/SiO_2 surface have highly oriented COF layers aligned parallel to the substrate surface. Moreover, this liquid–solid growth process affords TAPB-PDA COF thin films with p-type charge transport having a transconductance of 10 μS at a gate voltage of −0.9 V in an OECT device structure.

Received 15th November 2023,
Accepted 29th February 2024

DOI: 10.1039/d3nr05798d

rsc.li/nanoscale

Introduction

Covalent organic frameworks (COFs) are an extraordinarily versatile class of organic materials exhibiting nanoscale porosity, large-scale crystallographic ordering, and offering a vast library of prospective monomers and linker chemistries.[1–3] The synthesis of these materials is most commonly performed using solvothermal techniques to generate highly crystalline powders. However, in applications requiring thin films, the fine control of thickness, morphology, crystallographic orientation, composition and structure is necessary to drive the desired properties of interest.[4,5] Current approaches towards obtaining high-quality COF thin films directly on solid substrates include bottom-up methods such as solvothermal synthesis,[6–23] vapor-assisted conversion,[24] and continuous flow.[25–27] These bottom-up growth techniques are many times referred to as interfacial synthesis, where monomers are forced to react at liquid–liquid, liquid–solid, or liquid–air interfaces resulting in large grain sizes (micron-scale in some cases)[28] and some degree of controllable film thicknesses.[29–31] COF thin films synthesized using these methods typically result in films with varying degrees of crystallographic orientation on a wide variety of substrates.

In a typical liquid–liquid interfacial imine COF growth procedure, the reagents remain in separate immiscible phases in some cases featuring the acid catalyst in the aqueous phase separate from the amine and aldehyde monomers[32] while in

[a]*Materials and Manufacturing Directorate, Air Force Research Laboratory, Wright-Patterson Air Force Base, Ohio 45433, USA. E-mail: Nicholas.Glavin.1@us.af.mil*
[b]*UES, Inc., Beavercreek, Ohio 45432, USA*
[c]*Cornell High Energy Synchrotron Source, Cornell University, Ithaca, New York 14853, USA*
[d]*Department of Chemistry and the Materials Research Center, Northwestern University, Sheridan Road, Evanston, IL 60208, USA*
[e]*Department of Chemical and Materials Engineering, University of Dayton, Dayton, Ohio 45469, USA*
[f]*Department of Materials Science and NanoEngineering, Rice University, Houston, Texas 77005, USA*
[g]*Department of Materials Science and Engineering, Cornell University, Ithaca, New York 14853, USA*
[h]*School of Materials Science and Engineering, Georgia Institute of Technology, Atlanta, Georgia 30332, USA*
† Electronic supplementary information (ESI) available. See DOI: https://doi.org/10.1039/d3nr05798d

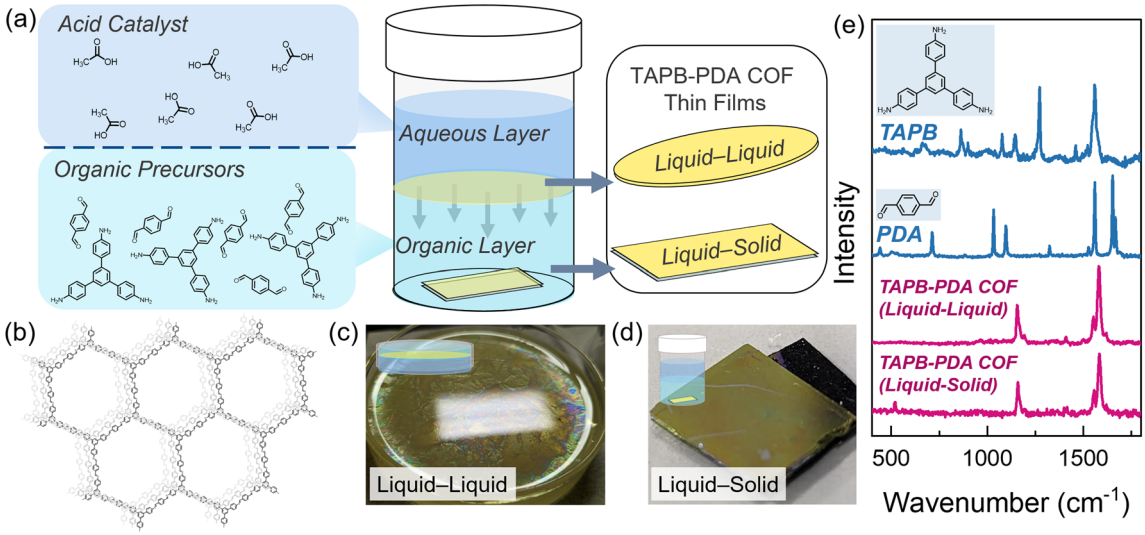

Fig. 1 Liquid–liquid (LL) and liquid–solid (LS) COF growth. (a) LL and LS COF film growth setups; (b) structure of TAPB-PDA COF; (c) photograph of LL growth of COF film in a Petri dish; (d) photograph of LS growth of COF film on silicon substrate; (e) Raman spectra of precursors (TAPB and PDA) depicted in blue and TAPB-PDA COF film from LL and LS growth depicted in dark pink (silicon substrate peak at 520 cm^{-1}).

others the amine monomer and acid catalyst are in the same phase.[33] These arrangements both force a majority of the COF thin film to form at the liquid–liquid interface where the highest concentration of all reagents meet. Recent work by Mahato *et al.*[34] reveals that films can be synthesized both at this interface and on a solid surface in the organic layer through residual crystallization using a liquid–liquid set up. In their work, a diamine linker is placed in the top aqueous phase and reacts at the interface with trialdehyde linkers from the bottom organic phase to form a COF film. However, their work also demonstrates that the diamine linker is capable of diffusing into the organic layer and reacting with the trialdehyde near the surface of a substrate placed at the bottom. As a result, COF films can also form at this liquid–solid interface. Importantly, due to the slow diffusion of the monomers, the film formed at the liquid–solid interface exhibits a higher degree of crystallinity than the film formed at the liquid–liquid interface.[29]

Here, we utilize the liquid–solid growth technique to explore morphology and crystallographic orientation, two critical thin film properties for future applications, of imine COF films grown directly onto substrates (Fig. 1a). We demonstrate that this residual/liquid–solid method produces films with consistent thicknesses on the nanometer level which could be used for future electronic and optical device fabrication. This is in contrast to films grown at the liquid–liquid interface which produces micron level variations in thickness and can suffer from poor adhesion to some substrates. Additionally, we also show that the acid concentration strongly affects the morphology of the liquid–solid TAPB-PDA COF films with those most smooth achieved when the molarity of the acid in the aqueous phase is kept within a certain range. Furthermore, we show that optimization of the growth time produces sub-20 nm films with nanometer level smoothness in just 30 minutes and illustrate that film orientation is strongly dependent upon growth conditions. These studies are culminated with a demonstration showing optimal films are semiconducting and function as the channel in organic electrochemical transistors.

Nicholas R. Glavin

Dr Nicholas Glavin, a Senior Materials Engineer at the Air Force Research Laboratory (AFRL), has dedicated his early career research towards nanotechnology solutions for electronics, sensing, and defense-related applications. Holding a PhD in Mechanical Engineering from Purdue University and a MS/BS in Chemical Engineering from the University of Dayton, he is recognized for his expertise in nanomaterial synthesis, processing and implementation into relevant applications. His research area focuses on two dimensional (2D) materials, 2D/3D integration, organic electronic materials, and heterostructures for microelectronics, chemical/biological sensors, and extreme environment electronics.

Results and discussion

COF film growth *via* liquid–liquid and liquid–solid synthesis

COF thin films were synthesized using the condensation reaction of 1,3,5-tris(4-aminophenyl) benzene (TAPB) (13 mg, 0.04 mmol, 1.0 eq.) and *p*-phthalaldehyde (PDA) (7.5 mg, 0.06 mmol, 1.5 eq.), which were added to a 20 mL scintillation

vial and dissolved in methylene chloride (8 mL) (Fig. 1a). Next, a Si/SiO_2 substrate approximately 1 cm^2 was placed at the bottom of the vial. Then 8 mL of aqueous acetic acid (from 1 M to 10 M) was slowly syringed on top of the organic layer ensuring minimal disruption of the solvent–solvent interface. TAPB-PDA COF (structure shown in Fig. 1b) film formation through liquid–liquid (LL) growth and liquid–solid (LS) growth began almost instantly upon adding the aqueous layer containing the catalyst (shown in Fig. 1c and d). After removing the substrate for LS growth, it was placed in a vial of acetone and briefly sonicated (<5 s) to remove large particulates from the surface. Chemical characterization of the TAPB-PDA COF grown both through the LL and LS methods was carried out using Raman spectroscopy. Fig. 1e reports the Raman spectra of the monomer powders (PDA and TAPB) as well as the TAPB-PDA COF from both growth methods. The Raman peaks associated with the starting monomers were not present in the final COF thin films. Expected C=N stretching modes at 1590 and 1560 cm^{-1} and aromatic stretching modes for C–H at 1160 cm^{-1} are instead present, indicating conversion of the monomer precursors to an imine network.[35] Additionally, the Raman spectra of the LL and LS TAPB-PDA COF both showed the same spectra with the exception of the SiO_2/Si substrate feature at 520 cm^{-1} in the case of the thinner films from LS growth. Scanning electron microscopy (SEM) and energy dispersive X-Ray spectroscopy (EDX) was used to distinguish the LS film from the substrate. Areas containing the film had a higher percentage of carbon, while areas with only substrate had a higher percentage of silicon (further information in Fig. S3 and S4†).

To fully characterize the TAPB-PDA COF (LS) and investigate the porosity, transmission electron microscopy (TEM) was conducted. An amorphous carbon coated TEM grid was attached to a silicon substrate and introduced to the LS growth setup. Afterwards, it was briefly sonicated to remove excess material and used for analysis. Fig. 2 shows a close-up real-space TEM image of the TAPB-PDA COF grown directly onto the TEM grid. The top right corner of Fig. 2 shows the corresponding fast Fourier transform (FFT) of the selected area indicating the periodicity originating from the [100] plane of the crystalline porous structure. It can clearly be noted that the pore size approaches 3.3 nm which closely matches previous literature reports of the same COF[36] (see Fig. S5 and S6 in the ESI† for additional TEM images).

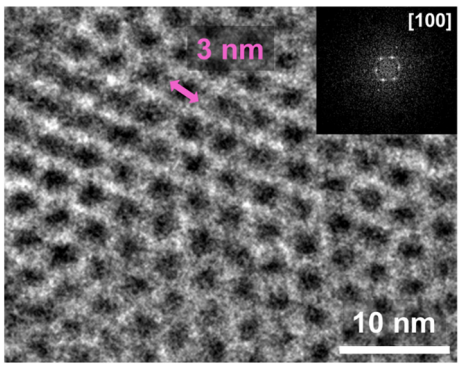

Fig. 2 TEM Image and resulting FFT of liquid–solid TAPB-PDA COF. Magenta arrow indicates pore distance of 3 nm and FFT shows the periodicity of the [100] plane arising from the porous crystalline structure.

Acid concentration dependent film morphology with liquid–solid growth on substrate

To study the effect of acid concentration on liquid–solid (LS) film growth, COF thin films were grown on Si/SiO_2 wafers using a range of molarities of acetic acid (AcOH) in the aqueous layer. Shown in Fig. 3a, the higher concentrations of

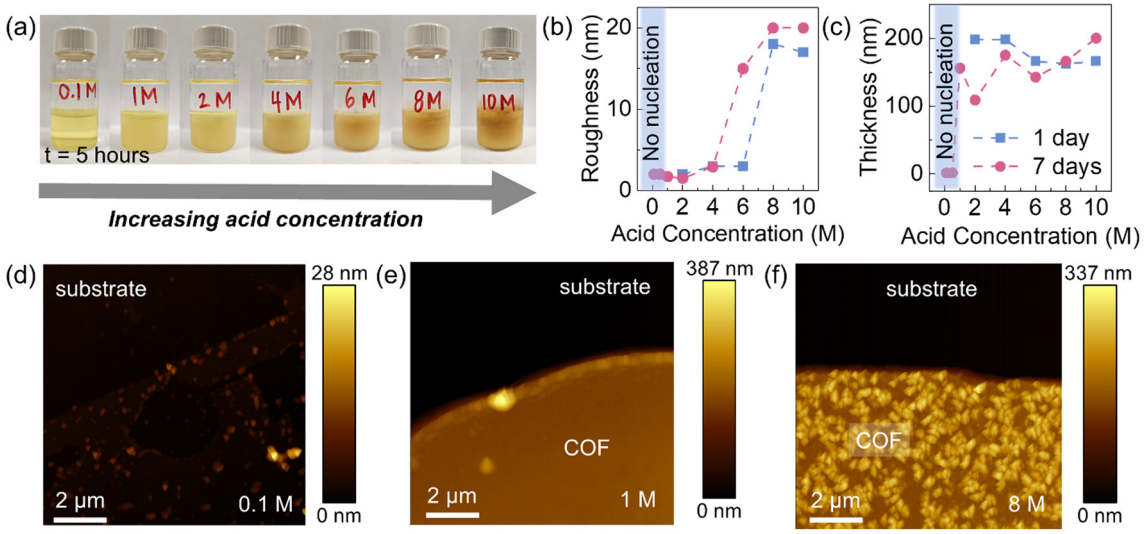

Fig. 3 Liquid–solid film roughness and thickness as a function of acid concentration. (a) Photographs exhibiting COF growth set up with range of different acid concentrations (0.1 M to 10 M AcOH) after 5 hours; (b) graph of acid molarity and film roughness (nm); (c) graph of acid molarity and film thickness (nm); (d) AFM of substrate after 7 days with 0.1 M AcOH solution used in aqueous layer (no nucleation); (e) AFM of smooth COF thin film formed on substrate after 7 days with 2 M AcOH solution used in aqueous layer (film thickness = 185 nm, R_q = 2 nm); (f) AFM of rough COF film formed on substrate after 1 day with 8 M AcOH solution used in aqueous layer (film thickness = 200 nm, R_q = 20 nm).

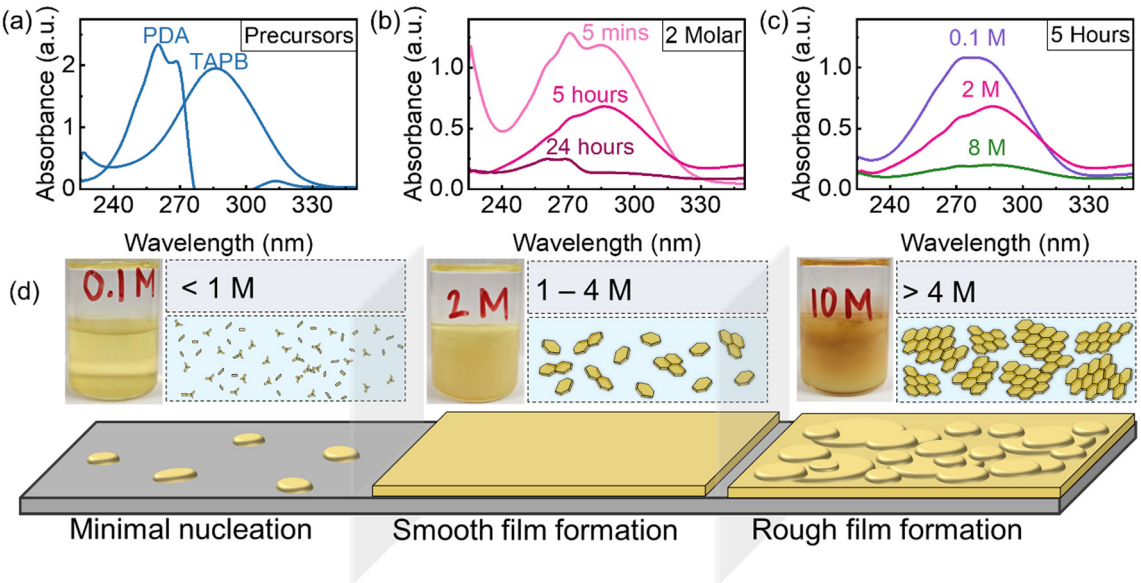

Fig. 4 Proposed growth mechanism of liquid–solid (LS) COF film under different acid concentrations. UV-Vis absorption data for (a) precursors PDA and TAPB, (b) organic layer at 5 minutes, 5 hours, and 24 hours after reaction with 2 M acetic acid in aqueous layer (c) organic layer after 5 hours with acid molarities of 0.1, 2, and 8; (d) schematic of LS film formation as a result of acid concentration. Top left of each section shows photograph of reaction after 5 hours, top right of each section shows molarity range and resulting COF formation in organic layer.

acetic acid showed the visible presence of particulates in the bottom organic layer after 5 hours, while the lowest acid concentration showed minimal color change and the absence of particulates in the organic solution (see additional Raman analysis in Fig. S7 and time-lapse photographs in Fig. S8 in the ESI†). To investigate the influence of acid molarity on film morphology, atomic force microscopy (AFM) was used to evaluate both surface roughness and film thickness (Fig. 3b and c). Roughness analysis of the films grown both over 1 day and 7 days at varying acetic acid molarities reveals that the acid concentration strongly affects the resultant surface roughness of the LS COF thin films (Fig. 3b). AFM shows that acetic acid molarities below 1 M result in very little nucleation or growth, as the catalyst concentration appears insufficiently high to initiate imine formation (Fig. 3d). AFM also shows that with acid concentrations between 1 and 4 M, complete film formation with nanoscale roughness less than 4 nm is achieved, indicating ideal conditions for smooth and continuous TAPB-PDA COF film synthesis in this study (Fig. 3e). Additional SEM analysis of this LS growth condition is also included in Fig. S9 in the ESI.† AFM shows that at higher acetic acid concentrations, the surface roughness dramatically increases as particulates ranging from 100–200 nm in area and approximately 15 nm in height form readily on the COF film (Fig. 3f). Film thicknesses for experiments range between 150–200 nm with minimal difference between 1 day and 7 day growth, presumably due to the formation of the interfacial film between liquid–liquid interfaces.

Reaction progression. To further understand the growth reaction mechanism and progression, UV-Vis spectroscopy was used to explore the change in optical properties of the organic layer over time (see Fig. 4a). To perform this experiment, an aliquot was removed from the middle of the organic layer in the COF growth setup and diluted by 1000× for analysis. The UV-Vis spectrum of the isolated monomers is shown in Fig. 4a, which exhibits several unique peaks between 240 and 330 nm associated with both PDA and TAPB in solution. Fig. 4b shows the optical absorption spectrum of the organic layer at various times with 2 M acetic acid in the aqueous layer, with evidence of the present monomers reducing substantially when approaching 24 hours. The rate of monomer consumption is strongly dependent upon the acid concentration,[37] as shown in Fig. 4c with nearly all monomers consumed within 5 hours in the case of 8 M acetic acid concentration.

The proposed thin film growth mechanism for acid-dependent growth of the TAPB-PDA COF (LS) is shown in Fig. 4d. For concentrations below 1 M, minimal film formation is observed, due to the limited concentration of COF oligomers present in solution and insufficient concentration of the acid to catalyze imine formation. However, when the acid concentration is between 1 M and 4 M, a generally smooth film is observed. This is due to the fact that sufficient acid has diffused across the liquid–liquid interface enabling a reaction between the monomers, and thus driving the coalescence of crystalline domains. As a result, it is proposed that adequate, yet small-sized COF oligomers are present in the solution throughout and can therefore deposit and react onto the substrate. This produces accelerated COF growth in the lateral direction while limiting variations in thickness to less than 2 nm. Chen *et al.* describes a similar phenomenon of organic film growth where through Ostwald ripening, adjacent thin islands merge as a result of their high surface-area-to-volume

ratio and mobility on SiO_2, leading to coalescence in the lateral direction. However, when the growing domain was isolated, it underwent a self-confined layer growth mode, leading to increase in the vertical direction.[38] The film morphology was found to be related to the percentage of molecules contained in islands greater than the critical island size, and thus explains the observed film roughening shown in Fig. 3f. When the acid concentration is greater than 4 M, a rough film is formed presumably due to a large presence of the acid catalyst that has diffused across the liquid–liquid interface causing rapid uncontrolled imine bond formation between the monomers resulting large COF oligomers (Fig. 4d, right). These oligomers deposit onto the substrate surface and grow vertically to form a roughened film with large COF clusters throughout and thus restricts smooth film formation in the lateral direction. Similarly, an increase in film roughness has been observed in vapor–solid COF growth *via* chemical vapor deposition (CVD) at lower growth temperatures.[39] In this case, film morphology and growth in the lateral *versus* vertical direction appear to be ultimately affected by the concentration of reacted monomers in solution.[38,40]

Time dependent film morphology. A major advantage to bottom-up COF growth using the techniques described herein is the ability to control film thickness. To probe if this method can be used to produce even thinner films, while retaining the overall smoothness, early liquid–solid (LS) growth film experiments were conducted. Fig. 5a–f shows several AFM and SEM images of early-stage COF growth on Si/SiO_2 substrates. These results reveal that patchy COF films are deposited onto the substrate in as little as three minutes, as indicated by the AFM and SEM images shown in Fig. 5a and b, with cracks and uncoalesced film areas. At 30 minutes of growth time, smooth and continuous films can be observed which exhibit a more uniform film coverage with under 2 nm in film roughness throughout most parts (Fig. 5c and d). After 100 minutes of growth time, a slight increase in roughness can be observed where Fig. 5e and f show the occurrence of nanoscale islands/clusters on top of a smooth film. It is evident that COF film formation first takes place on the substrate through nonclassical nucleation,[38] and grows outwards until a smooth and continuous film is formed.[41] Afterwards, islands of COF begin to appear and extend upward,[42] justifying the Ostwald ripening mentioned previously. All COF films in this analysis appear under 60 nm in height. It should be noted however that early-stage growth does not produce wafer scale COF films and instead results in inhomogeneous growth throughout the substrate. Fig. 5 summarizes the morphology of a majority of the COF film (LS) on the substrate but does not adequately define the entirety of the film. This is in comparison to the LS growths lasting 24 hours or longer, which are capable of producing uniform and wafer scale films of greater thickness throughout. See Fig. S10–S15 in the ESI† for additional AFM and SEM images.

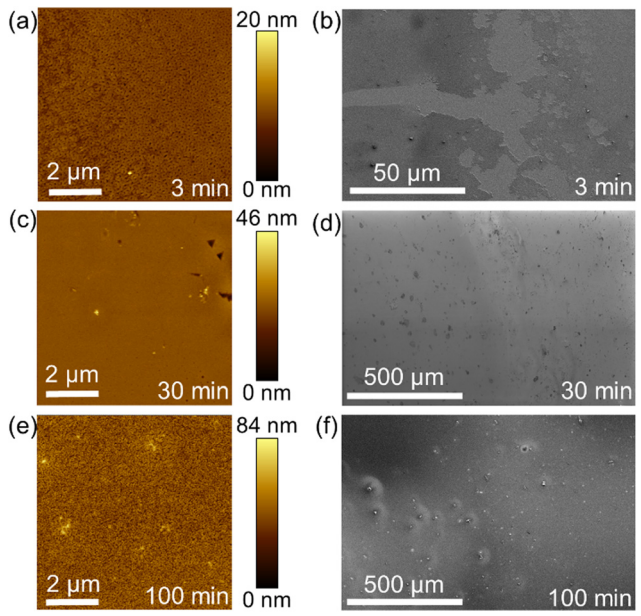

Fig. 5 Time dependency and early liquid–solid film formation. (a) AFM image of uncoalesced film growth after 3 minutes (film thickness = 20 nm, R_q = 5 nm); (b) SEM image of uncoalesced film after 3 minutes; (c) AFM image of coalesced smooth film after 30 minutes (film thickness = 37 nm, R_q < 2 nm); (d) SEM image of coalesced film after 30 minutes; (e) AFM image of rougher film formation after 100 minutes (film thickness = 55 nm, R_q = 6 nm); (f) SEM image of rougher film formation after 100 minutes.

Orientation control

For future applications in electronic devices including sensors, ambipolar electronics, and transistors of different types, the control and manipulation of the COF film crystal orientation is critical. To study the influence of growth conditions on both the crystallinity and orientation of the TAPB-PDA COF thin films, grazing-incidence wide-angle X-ray scattering (GIWAXS) was performed. Prior to this analysis, the films underwent an annealing and subsequent activation step used to remove solvent and impurities from the pores[43] (see further details on page S4 in the ESI†). The resulting scattering images and corresponding plots are shown in Fig. 6. Several different films were analyzed (Fig. 6a–d), including both liquid–solid (LS) growth and liquid–liquid (LL) growth, to understand the different effects of specific growth conditions. COF samples grown *via* LS growth on the substrate in both low and high acid concentrations exhibit a high degree of crystallinity with COF layers aligned parallel to the substrate surface (Fig. 6f, top). This level of crystallinity and orientation is retained even when the thickness of the COF film is increased after subjecting it to the same conditions again (Fig. 6c). More information on this regrowth experiment can be found in Fig. S16 and S17 in the ESI.† This preferred orientation is indicated by the vertical peaks that appear between 0.18 $Å^{-1}$ and 0.21 $Å^{-1}$ in Fig. 6a–c which correspond to the [100] of the hexagonal lattice.[44–46] Using Bragg's law, the *d*-spacing for these planes was determined from the peak position, q_{max}, using the following equation:

$$d_{Bragg} = \frac{2\pi}{q_{max}}$$

The *d*-spacings are 32.2 Å, 32.4 Å, 32.2 Å, and 33.2 Å for Fig. 6a–d, respectively which matches previous literature

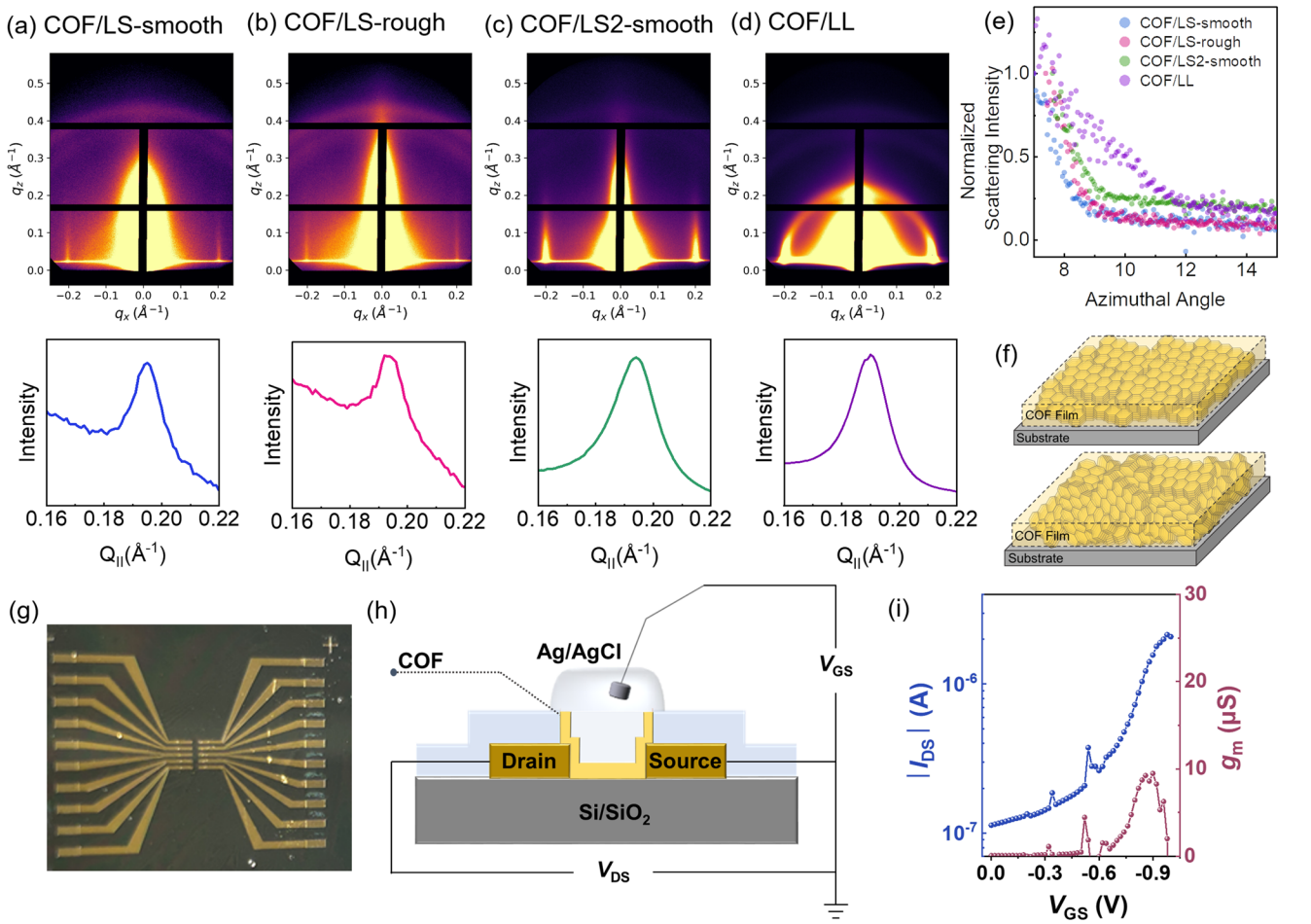

Fig. 6 Film orientation with grazing-incidence wide-angle X-Ray Scattering and OECT performance. (a–d) GIWAXS patterns and azimuthal integration for liquid–solid (LS) and liquid–liquid (LL) growth TAPB-PDA COFs; (a) COF/LS-smooth (110 nm thickness), growth conditions: 2 molar, 7 days; (b) COF/LS-rough (160 nm thickness), growth conditions: 8 M AcOH, 7 days; (c) COF/LS2-smooth, growth conditions: 1 M AcOH, 7 days, resubject to 1 M AcOH, 3 days; (d) COF/LL, growth conditions: 0.1 M AcOH, 3 days in Petri dish (e) *I vs.* χ plot for a–d; (f) parallel orientation (top) *versus* mixed orientation (bottom) schematic; (g) photo image of transistor devices; (h) schematic depiction of LS OECT device cross-section; (i) Transfer curve (V_{GS} from 0 V to −0.95 V and V_{DS} = −0.7 V) of a TAPB-PDA OECT with a $W \times L$ of 500 μm × 10 μm.

reports for the same COF.[47,48] Additionally the PXRD data from the COF (LL) in Fig. S1† was converted to *I vs. Q*. The obtained pattern matches the 1D projection of the collected GIWAXS data from the COF (LS) (see Fig. S18 in the ESI†).

The parallel orientation of the COF relative to the surface of the substrate is a result of a few contributing factors of this unique interfacial growth setup. Firstly, the slow diffusion of the acetic acid across the liquid–liquid interface controls the precise deposition and therefore lateral growth of the COF with initial preferential parallel orientation. Also, the COF formed at the liquid–liquid interface between the aqueous and organic layers likely plays a role in continuing to slow and control the acid diffusion. This is evident for the LS growth based on the observed morphological features that occur when the acid concentration is changed as well as the early growth experiments depicted in the AFM images of Fig. 3 and 5, respectively. Secondly, the preference for parallel orientation is retained as the COF film continues to grow in the vertical direction. This is likely due to the favorable π–π interactions between the initial layers of COF and the layers that begin to form on top.[49] This has been previously observed in works which describe the growth of COFs on single-layer graphene (SLG) and show that the thickness and uniformity of orientated films are also dependent on the underlying substrate.[7,50] This is also evident in Fig. 6c, which shows that a COF film (LS) which was resubjected to the same growth conditions increases in thickness but retains parallel orientation.

Comparatively, the scattering image of the LL growth shown in Fig. 6d depicts a semicircle with bright spots at the edges and top, suggesting randomly oriented crystallites (Fig. 6f, bottom), similar to a powder.[27] The azimuthal integration for each scattering image is shown below in Fig. 6. Fig. 6e shows the scattering intensity *versus* χ plots and distribution around the azimuth for COF samples in Fig. 6a–d. All LS growth samples (Fig. 6e; blue, pink, green) show a sharp decay in the azimuthal scattering from the [100] peak, indicating that the

planes are vertically well-aligned with correlations in the direction parallel to the surface of the substrate. The LL film (purple) is the outlier in this graph with a distribution of mixed orientations of the [100] planes relative to the surface of the substrate. This is likely due to the dynamic nature of the liquid–liquid interface, which aids in COF crystallization but does not cause any preferential alignment. Previous work has shown that a polymer is required to guide the ordering and alignment of COF crystallization at a liquid–air interface.[28]

Semiconductor performance

Finally, we investigated TAPB-PDA COF films synthesized *via* the liquid–solid method as prospective semiconductor channels in organic electrochemical transistors (OECTs) (Fig. 6g). Organic electrochemical transistors operate by transducing a small gate voltage potential (V_{GS}) into a channel current (I_{DS}) between source and drain electrodes.[51,52] The optical image of the OECTs array fabricated in this study is shown in Fig. 6h while device fabrication process is shown in the ESI (Fig. S19†). These OECTs have a channel dimension of 500 × 10 μm^2 (width × length) and details can be found in the ESI.† The transfer curve (I_{DS}–V_{GS}) shown in Fig. 6i indicates a p-type (hole transport) operation. These devices show typical gate modulation of the channel current over a gate voltage range from 0 V to −0.95 V. The transconductance (g_m), extracted from the slope of the transfer curve is a critical parameter for using an OECT as an amplifier. In this work, a maximum g_m of approximately 9.5 μS at a gate voltage of −0.9 V is measured. Note, the low current/transconductance is expected considering the low semiconductor mass in the channel of these devices. Our TAPB-PDA COF films are quite thin (≈25 nm) and have very low density (0.38 g cm^{-3})[53] compared to the typical conjugated organic polymers (≈100 nm thick, density > 1 g cm^{-3}) commonly used in OECTs.[54–56] Additionally, the hydrophobic nature of the COF channel[57] may cause limited volumetric capacitance of electrochemical transistors operated in aqueous electrolyte. Future investigations of COF-based electrochemical transistors will focus on the optimization of COF film hydrophilicity,[58] which can be affected by crystallinity and surface area, and enhancement of the semiconducting monomer components.

Conclusions

Ensuring strict control of crystallographic orientation and morphology during COF thin film growth remains a crucial parameter for implementation of these exciting materials into electronic and photonic applications. In this study, an interfacial setup was used to synthesize COF thin films both at the liquid–liquid (LL) and liquid–solid (LS) interfaces at room temperature. The acetic acid concentration was found to strongly affect film morphology of the LS growth, where concentrations of 1–4 M enabled the formation of smooth films (<200 nm in thickness, 1–2 nm roughness) after 24 hours. Early growth experiments showed the evolution of LS film formation from patchy to smooth and uniform films and then to rougher and thicker films at longer growth times. GIWAXS studies highlight the difference in orientation between the LS growth and LL growth methods, where LS growth showed a high degree of parallel alignment to the surface of the substrate and LL growth showed mixed orientation. Finally, charge transport measurements of OECTs fabricated from the LS growth method demonstrate that the present COF films are a p-type semiconductor. In future applications utilizing transistors, optoelectronic devices, and catalytic films made from semiconducting COFs, understanding the pore alignment and crystal structure in COF thin films will be important as electronic properties are governed by a multitude of factors. Future work linking thin film synthesis to controllable electronic properties of COFs will be significant as these exciting materials continue to push the boundaries of wafer-scale organic electronic materials and potential device configurations.

Author contributions

D. D. B., L. T., A. Re., Q. F., and C. M. performed COF synthesis and characterization. D. D. B., K. P., H. K. performed and evaluated GIWAXS experiments. A. Ru. performed SEM and surface characterization. C. H. performed TEM analysis. Y. Y. fabricated and evaluated OECT devices. D. D. B., T. J. M., A. F., L. D., L. B., Y. Z., J. L., J. K. and N. G. led the supervision of experiments and manuscript preparation and drafting.

Conflicts of interest

There are no conflicts of interest.

Acknowledgements

D. D. B., L. T., L. B., and N. G. acknowledge financial support from The Air Force Office of Scientific Research (AFOSR) grant number 23RXCOR011. A. F. and T. J. M. gratefully acknowledge financial support by AFOSR grant FA9550-22-1-0423. This material is based on research sponsored by AFRL under agreement number FA8650-22-2-5200. The U.S. Government is authorized to reproduce and distribute reprints for Governmental purposes notwithstanding any copyright notation thereon.

References

1 P. Côté, A. I. Benin, N. W. Ockwig, M. O'Keeffe, A. J. Matzger and O. M. Yaghi, *Science*, 2005, **310**, 1166–1170.
2 F. Haase and B. V. Lotsch, *Chem. Soc. Rev.*, 2020, **49**, 8469–8500.
3 S. Kandambeth, K. Dey and R. Banerjee, *J. Am. Chem. Soc.*, 2019, **141**, 1807–1822.

4 L. K. Beagle, Q. Fang, L. D. Tran, L. A. Baldwin, C. Muratore, J. Lou and N. R. Glavin, *Mater. Today*, 2021, **51**, 427–448.
5 J. L. Fenton, D. W. Burke, D. Qian, M. Olvera de la Cruz and W. R. Dichtel, *J. Am. Chem. Soc.*, 2021, **143**, 1466–1473.
6 E. L. Spitler, B. T. Koo, J. L. Novotney, J. W. Colson, F. J. Uribe-Romo, G. D. Gutierrez, P. Clancy and W. R. Dichtel, *J. Am. Chem. Soc.*, 2011, **133**, 19416–19421.
7 J. W. Colson, A. R. Woll, A. Mukherjee, M. P. Levendorf, E. L. Spitler, V. B. Shields, M. G. Spencer, J. Park and W. R. Dichtel, *Science*, 2011, **332**, 228–231.
8 E. L. Spitler, J. W. Colson, F. J. Uribe-Romo, A. R. Woll, M. R. Giovino, A. Saldivar and W. R. Dichtel, *Angew. Chem., Int. Ed.*, 2012, **51**, 2623–2627.
9 D. D. Medina, V. Werner, F. Auras, R. Tautz, M. Dogru, J. Schuster, S. Linke, M. Döblinger, J. Feldmann, P. Knochel and T. Bein, *ACS Nano*, 2014, **8**, 4042–4052.
10 R. DeBlase, K. Hernández-Burgos, K. E. Silberstein, G. G. Rodríguez-Calero, R. P. Bisbey, H. D. Abruña and W. R. Dichtel, *ACS Nano*, 2015, **9**, 3178–3183.
11 X. Gou, Q. Zhang, Y. Wu, Y. Zhao, X. Shi, X. Fan, L. Huang and G. Lu, *RSC Adv.*, 2016, **6**, 39198–39203.
12 D. Medina, M. L. Petrus, A. N. Jumabekov, J. T. Margraf, S. Weinberger, J. M. Rotter, T. Clark and T. Bein, *ACS Nano*, 2017, **11**, 2706–2713.
13 L. D. Tran, B. J. Ree, A. Ruditskiy, L. K. Beagle, R. C. Selhorst, D. D. Bhagwandin, P. Miesle, L. F. Drummy, M. F. Durstock, R. Rao, H. Koerner, N. R. Glavin and L. A. Baldwin, *Adv. Mater. Interfaces*, 2023, **10**, 2300042.
14 L. Ascherl, E. W. Evans, M. Hennemann, D. Di Nuzzo, A. G. Hufnagel, M. Beetz, R. H. Friend, T. Clark, T. Bein and F. Auras, *Nat. Commun.*, 2018, **9**, 3802.
15 T. Sick, A. G. Hufnagel, J. Kampmann, I. Kondofersky, M. Calik, J. M. Rotter, A. Evans, M. Döblinger, S. Herbert, K. Peters, D. Böhm, P. Knochel, D. D. Medina, D. Fattakhova-Rohlfing and T. Bein, *J. Am. Chem. Soc.*, 2018, **140**, 2085–2092.
16 M. Evans, A. Giri, V. K. Sangwan, S. Xun, M. Bartnof, C. G. Torres-Castanedo, H. B. Balch, M. S. Rahn, N. P. Bradshaw, E. Vitaku, D. W. Burke, H. Li, M. J. Bedzyk, F. Wang, J.-L. Brédas, J. A. Malen, A. J. H. McGaughey, M. C. Hersam, W. R. Dichtel and P. E. Hopkins, *Nat. Mater.*, 2021, **20**, 1142–1148.
17 S. Cai, B. Sun, X. Li, Y. Yan, A. Navarro, A. Garzón-Ruiz, H. Mao, R. Chatterjee, J. Yano, C. Zhu, J. A. Reimer, S. Zheng, J. Fan, W. Zhang and Y. Liu, *ACS Appl. Mater. Interfaces*, 2020, **12**, 19054–19061.
18 Y. Chen, H. Cui, J. Zhang, K. Zhao, D. Ding, J. Guo, L. Li, Z. Tian and Z. Tang, *RSC Adv.*, 2015, **5**, 92573–92576.
19 S. Lin, C. S. Diercks, Y.-B. Zhang, N. Kornienko, E. M. Nichols, Y. Zhao, A. R. Paris, D. Kim, P. Yang, O. M. Yaghi and C. J. Chang, *Science*, 2015, **349**, 1208–1213.
20 L. Ascherl, E. W. Evans, J. Gorman, S. Orsborne, D. Bessinger, T. Bein, R. H. Friend and F. Auras, *J. Am. Chem. Soc.*, 2019, **141**, 15693–15699.
21 S. Jhulki, A. M. Evans, X.-L. Hao, M. W. Cooper, C. H. Feriante, J. Leisen, H. Li, D. Lam, M. C. Hersam, S. Barlow, J.-L. Brédas, W. R. Dichtel and S. R. Marder, *J. Am. Chem. Soc.*, 2020, **142**, 783–791.
22 S. Zhang, Q. Yang, X. Xu, X. Liu, Q. Li, J. Guo, N. L. Torad, S. M. Alshehri, T. Ahamad, M. S. A. Hossain, Y. V. Kaneti and Y. Yamauchi, *Nanoscale*, 2020, **12**, 15611–15619.
23 S. Zhang, W. Xia, Q. Yang, Y. Valentino Kaneti, X. Xu, S. M. Alshehri, T. Ahamad, Md. S. A. Hossain, J. Na, J. Tang and Y. Yamauchi, *Chem. Eng. J.*, 2020, **396**, 125154.
24 D. Medina, J. M. Rotter, Y. Hu, M. Dogru, V. Werner, F. Auras, J. T. Markiewicz, P. Knochel and T. Bein, *J. Am. Chem. Soc.*, 2015, **137**, 1016–1019.
25 R. P. Bisbey, C. R. DeBlase, B. J. Smith and W. R. Dichtel, *J. Am. Chem. Soc.*, 2016, **138**, 11433–11436.
26 Y. Yang, C. Schäfer and K. Börjesson, *Chem*, 2022, **8**, 2217–2227.
27 D. D. Bhagwandin, J. H. Dunlap, L. D. Tran, A. Reidell, D. Austin, A. A. Putnam-Neeb, M. Loveday, R. Rao, L. A. Baldwin and N. R. Glavin, *CrystEngComm*, 2024, **26**, 27–31.
28 Z. Ou, B. Liang, Z. Liang, F. Tan, X. Dong, L. Gong, P. Zhao, H. Wang, Y. Zou, Y. Xia, X. Chen, W. Liu, H. Qi, U. Kaiser and Z. Zheng, *J. Am. Chem. Soc.*, 2022, **144**, 3233–3241.
29 S. Kim and H. C. Choi, *ACS Omega*, 2020, **5**, 948–958.
30 Q.-W. Meng, S. Wu, M. Liu, Q. Guo, W. Xian, X. Zuo, S. Wang, H. Yin, S. Ma and Q. Sun, *Sci. Adv.*, 2023, **9**, eadh0207.
31 T. Zhang, X. Fu, C. Wu, F. J. Tan, Y. Liu and S. Xia, *J. Environ. Chem. Eng.*, 2021, **9**, 106807.
32 M. Matsumoto, L. Valentino, G. M. Stiehl, H. B. Balch, A. R. Corcos, F. Wang, D. C. Ralph, B. J. Mariñas and W. R. Dichtel, *Chem*, 2018, **4**, 308–317.
33 K. Dey, M. Pal, K. C. Rout, S. H. Kunjattu, A. Das, R. Mukherjee, U. K. Kharul and R. Banerjee, *J. Am. Chem. Soc.*, 2017, **139**, 13083–13091.
34 K Mahato, S. Bag, H. S. Sasmal, K. Dey, I. Giri, M. Linares-Moreau, C. Carbonell, P. Falcaro, E. B. Gowd, R. K. Vijayaraghavan and R. Banerjee, *J. Am. Chem. Soc.*, 2021, **143**, 20916–20926.
35 S. A. Ahmed, Q. Liao, Q. Shen, M. M. F. Ashraf Baig, J. Zhou, C. Shi, P. Muhammad, S. Hanif, K. Xi, X. Xia and K. Wang, *Chem. – Eur. J.*, 2020, **26**, 12996–13001.
36 D. Zhu, J.-J. Zhang, X. Wu, Q. Yan, F. Liu, Y. Zhu, X. Gao, M. M. Rahman, B. I. Yakobson, P. M. Ajayan and R. Verduzco, *Chem. Sci.*, 2022, **13**, 9655–9667.
37 R. L. Li, N. C. Flanders, A. M. Evans, W. Ji, I. Castano, L. X. Chen, N. C. Gianneschi and W. R. Dichtel, *Chem. Sci.*, 2019, **10**, 3796–3801.
38 H. Chen, M. Li, Z. Lu, X. Wang, J. Yang, Z. Wang, F. Zhang, C. Gu, W. Zhang, Y. Sun, J. Sun, W. Zhu and X. Guo, *Nat. Commun.*, 2019, **10**, 3872.
39 J. P. Daum, A. Ajnsztajn, S. A. Iyengar, J. Lowenstein, S. Roy, G. Gao, E. H. R. Tsai, P. M. Ajayan and R. Verduzco, *ACS Nano*, 2023, **17**, 21411–21419.

40 D. Cui, Y. Fang, O. MacLean, D. F. Perepichka, F. Rosei and S. Clair, *Chem. Commun.*, 2019, **55**, 13586–13589.
41 H. S. Sasmal, A. Halder, S. H. Kunjattu, K. Dey, A. Nadol, T. G. Ajithkumar, P. R. Bedadur and R. Banerjee, *J. Am. Chem. Soc.*, 2019, **141**, 20371–20379.
42 D. D. Medina, V. Werner, F. Auras, R. Tautz, M. Dogru, J. Schuster, S. Linke, M. Döblinger, J. Feldmann, P. Knochel and T. Bein, *ACS Nano*, 2014, **8**, 4042–4052.
43 D. Zhu and R. Verduzco, *ACS Appl. Mater. Interfaces*, 2020, **12**, 33121–33127.
44 J. W. Colson, A. R. Woll, A. Mukherjee, M. P. Levendorf, E. L. Spitler, V. B. Shields, M. G. Spencer, J. Park and W. R. Dichtel, *Science*, 2011, **332**, 228–231.
45 S.-L. Cai, Y.-B. Zhang, A. B. Pun, B. He, J. Yang, F. M. Toma, I. D. Sharp, O. M. Yaghi, J. Fan, S.-R. Zheng, W.-G. Zhang and Y. Liu, *Chem. Sci.*, 2014, **5**, 4693–4700.
46 M. Evans, A. Giri, V. K. Sangwan, S. Xun, M. Bartnof, C. G. Torres-Castanedo, H. B. Balch, M. S. Rahn, N. P. Bradshaw, E. Vitaku, D. W. Burke, H. Li, M. J. Bedzyk, F. Wang, J.-L. Brédas, J. A. Malen, A. J. H. McGaughey, M. C. Hersam, W. R. Dichtel and P. E. Hopkins, *Nat. Mater.*, 2021, **20**, 1142–1148.
47 J. Smith, A. C. Overholts, N. Hwang and W. R. Dichtel, *Chem. Commun.*, 2016, **52**, 3690–3693.
48 R. L. Li, A. Yang, N. C. Flanders, M. T. Yueng, D. T. Sheppard and W. R. Dichtel, Two Dimensional Covalent Organic Framework Solid Solutions, *J. Am. Chem. Soc.*, 2021, **143**, 7081–7087.
49 H. Wang, B. He, F. Liu, C. Stevens, M. A. Brady, S. Cai, C. Wang, T. P. Russell, T.-W. Tan and Y. Liu, *J. Mater. Chem. C*, 2017, **5**, 5090–5095.
50 B. Sun, C.-H. Zhu, Y. Liu, C. Wang, L.-J. Wan and D. Wang, *Chem. Mater.*, 2017, **29**, 4367–4374.
51 W. Huang, J. Chen, Y. Yao, D. Zheng, X. Ji, L.-W. Feng, D. Moore, N. R. Glavin, M. Xie, Y. Chen, R. M. Pankow, A. Surendran, Z. Wang, Y. Xia, L. Bai, J. Rivnay, J. Ping, X. Guo, Y. Cheng, T. J. Marks and A. Facchetti, *Nature*, 2023, **613**, 496–502.
52 Y. Yao, W. Huang, J. Chen, X. Liu, L. Bai, W. Chen, Y. Cheng, J. Ping, T. J. Marks and A. Facchetti, *Adv. Mater.*, 2023, **35**, 2209906.
53 Q. Fang, Z. Pang, Q. Ai, Y. Liu, T. Zhai, D. Steinbach, G. Gao, Y. Zhu, T. Li and J. Lou, *Proc. Natl. Acad. Sci. U. S. A.*, 2023, **120**, e2208676120.
54 P. R. Paudel, J. Tropp, V. Kaphle, J. D. Azoulay and B. Lüssem, *J. Mater. Chem. C*, 2021, **9**, 9761–9790.
55 M. Yamashita, C. Otani, H. Okuzaki and M. Shimizu, in 2011 *XXXth URSI General Assembly and Scientific Symposium*, IEEE, Istanbul, 2011, pp. 1–4.
56 C. M. Proctor, J. Rivnay and G. G. Malliaras, *J. Polym. Sci., Part B: Polym. Phys.*, 2016, **54**, 1433–1436.
57 D. Mullangi, S. Shalini, S. Nandi, B. Choksi and R. Vaidhyanathan, *J. Mater. Chem. A*, 2017, **5**, 8376–8384.
58 L. D. Tran, K. F. Presley, J. K. Streit, J. Carpena-Núñez, L. K. Beagle, T. A. Grusenmeyer, M. J. Dalton, R. A. Vaia, L. F. Drummy, N. R. Glavin and L. A. Baldwin, *Chem. Mater.*, 2022, **34**, 529–536.